Integrated GNSS Positioning and Attitude Determination for Structural Health Monitoring of Large-span Bridges

Xiangdong AN[1], **Xiaolin MENG**[1,*], **Liangliang HU**[2], **Yilin XIE**[3], and **Fan ZHANG**[4]

[1] *School of Instrument Science and Engineering, Southeast University, Nanjing, China, (xiangdong.ann@gmail.com, xiaolin_meng@seu.edu.cn)*

[2] *College of Architecture and Civil Engineering, Beijing University of Technology, Beijing, China, (huliangliang@emails.bjut.edu.cn)*

[3] *Jiangsu Hydraulic Research Institute, Nanjing, China, (xieyilin-1983@163.com)*

[4] *School of Civil Engineering, Southeast University, Nanjing, China, (seuzhangfan@outlook.com)*

[*] *corresponding author*

Abstract

Attaining accurate displacement and attitude information is essential for structural health monitoring of large-span bridges, as they provide critical information regarding the condition and stability of structures. Integrated determination of bridges displacement and attitude with Global Navigation Satellite System (GNSS) enables early detection of potential structural issues and produce a more effective maintenance plan for informed decision-making. The traditional method of GNSS-based attitude determination could be split into two steps: calculating the baseline first, and then deriving the attitude information from the baseline solution. This paper integrates GNSS positioning and attitude determination within one step. Firstly, this method combines the GNSS observations from multiple antennas located on the bridge, utilizes a unit quaternion to express the attitude, and parameterizes the displacement, attitude and carrier-phase ambiguities in one observation equation. Then, the Unscented Kalman Filter (UKF) is adapted to achieve the optimal estimation of the quaternion-based nonlinear systems. Finally, the double-differenced ambiguities between the stations are resolved to integers to improve the accuracy of positioning and attitude determination. As an example, this method is used to process the data gathered with the GeoSHM system on the Forth Road Bridge in the UK and the accuracy of the developed GNSS positioning and attitude determination method is evaluated and analyzed.

Keywords: GNSS integrated positioning and attitude determination, structural health Monitoring, unscented Kalman filter

Received: 9th December 2024. Revised: 7th February 2025. Accepted: 14th March 2025.

1 Introduction

Displacement and attitude are key indicators of bridge health conditions, essential for structural health monitoring (SHM). Monitoring these parameters helps assess operational states, detect anomalies, and ensure structural safety and durability. Global Navigation Satellite System (GNSS) enables real-time tracking of bridge displacement and attitude, allowing for continuous monitoring, prompt detection of risks, and timely interventions through a dedicated SHM network.

The primary GNSS-based method for bridge SHM is real-time kinematic (RTK), which leverages broadcast ephemeris and short-baseline (<3 km) double-difference observations to significantly mitigate errors such as orbital, clock, and atmospheric delays, enabling real-time, high-accuracy displacement monitoring of bridges (Meng et al., 2002; Brownjohn et al., 2004; Yu et al., 2014). However, the RTK positioning mode is currently limited to displacement monitoring and cannot effectively monitor real-time attitude changes in bridges.

GNSS attitude determination methods can be classified into two main categories: two-step methods and one-step methods. In the two-step method, dynamic baselines between receivers are first computed from raw observations, followed by the derivation of attitude information from these baselines (Tian et al., 2017; Liu et al., 2022). These methods require complex computations, such as matrix inversion, which pose singularity risks. Additionally, by separating positioning from attitude determination, they fail to capture the full cross-correlation between position and attitude parameters.

The one-step method leverages multiple GNSS receivers with a known geometric distribution on the structure, directly determining the three-dimentional (3D) position and attitude of the monitoring stations on the bridge. An approach to improve GNSS attitude determination lies in effectively utilizing baseline constraints (e.g., fixed distances between monitoring stations) to enhance ambiguity resolution success rates. Teunissen (2006) extended the classical Least Squares Ambiguity Decorrelation Adjustment (LAMBDA) method by introducing the Constrained LAMBDA (C-LAMBDA) method, incorporating baseline length constraints into the objective function to accelerate convergence and improve reliability. The Multivariate Constrained LAMBDA (MC-LAMBDA) method further adds "length + angle" constraints, significantly enhancing the model strength (Giorgi and Teunissen 2010). However, these methods primarily express attitude parameters as rotation matrices, imposing orthogonality constraints to ensure they belong to the SO(3) group, leading to computational complexity. Compared to rotation matrices, quaternions offer a minimal representation of attitude. Quaternion-based attitude determination using the Extended Kalman Filter (EKF) has demonstrated its effectiveness, particularly for aircraft and vehicle applications (Medina et al., 2020; An et al., 2024). However, these methods have yet to be explored to the real-time monitoring of large spatial structures such as bridges. While quaternions provide a compact representation for solving complex nonlinear systems, the integration of multiple GNSS antennas and IMU based on EKF has been investigated for Unmanned Aerial Vehicles (UAV) and vehicular applications (Eling et al., 2013a, 2013b).

In this paper, we developed a quaternion-based positioning and attitude determination method using an Unscented Kalman Filter (UKF; Julier et al., 2000; Wan and Van Der Merwe, 2000) for SHM applications, it is new to apply the GNSS integrated displacement and attitude determination method for bridge monitoring. The UKF offers specific advantages in this context due to its ability to handle nonlinearity more effectively. Unlike the EKF, which linearizes the system around a nominal state using first-order Taylor expansion, the UKF employs the unscented transform to approximate the state distribution. This approach allows it to capture higher-order moments better and provides increased robustness to nonlinearities. This research is designed to exploit the UKF's advantages in handling nonlinearities, which are essential in integrated GNSS positioning and attitude determination for SHM.

2 Mathematical models

2.1 Notations

The italic characters or symbols indicate scaler quantities or functions, e.g. c; boldface is used to denote a vector or matrix, e.g. $\mathbf{b}$ and $\mathbf{H}$; The matrix or vector transpose is indicated with a superscript $(\cdot)^\top$, e.g. $\mathbf{b}^\top$ and $\mathbf{H}^\top$. In this work, the Earth-Centered, Earth-Fixed (ECEF) of the global frame is abbreviated as e-frame. The bridge coordinate system is defined with the origin of the base station r_0, and its three axes point to Longitudinal-Lateral-Down of the bridge (Meng 2002). The local frame (n-frame) is defined with the origin r_1, and with three axes pointing to local North-East-Down. The body frame (b-frame) is defined with its origin at r_1, the right axis aligned with r_2 in the horizontal plane, the front axis perpendicular to the right axis within the horizontal plane, and the down axis pointing toward the local downward direction. The relationship between BCS, n-frame and b-frame are illustrated on Fig. 1.

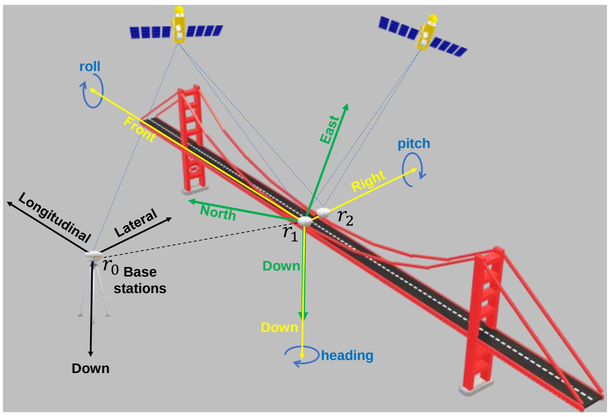

Figure 1 GNSS receivers' setup for SHM and the relationship between n-frame and b-frame.

2.2 Measurement model

Assuming we have one base station r_0 and two monitoring stations r_1, r_2 mounted on the middle span of the bridge, as marked in Fig. 1. The linearized double-differenced observation equations for baselines r_0r_1 and r_1r_2 between two satellites i, j on the l_{th} frequency are given as

$$\begin{cases} P_{r_0r_1,l}^{ij} = \rho_{r_0r_1}^{ij} + \mathbf{g}_{r_0}^{ij}\mathbf{R}_n^e\mathbf{b}_{r_0r_1}^n + \varepsilon\left(P_{r_0r_1,l}^{ij}\right) \\ P_{r_1r_2,l}^{ij} = \rho_{r_1r_2}^{ij} + \mathbf{g}_{r_1}^{ij}\mathbf{R}_n^e\mathbf{b}_{r_1r_2}^n + \varepsilon\left(P_{r_1r_2,l}^{ij}\right) \\ L_{r_0r_1,l}^{ij} = \rho_{r_0r_1}^{ij} + \mathbf{g}_{r_0}^{ij}\mathbf{R}_n^e\mathbf{b}_{r_0r_1}^n + \lambda_l N_{r_0r_1,l}^{ij} + \varepsilon\left(L_{r_0r_1,l}^{ij}\right) \\ L_{r_1r_2,l}^{ij} = \rho_{r_1r_2}^{ij} + \mathbf{g}_{r_1}^{ij}\mathbf{R}_n^e\mathbf{b}_{r_1r_2}^n + \lambda_l N_{r_1r_2,l}^{ij} + \varepsilon\left(L_{r_1r_2,l}^{ij}\right) \end{cases}, \quad (1)$$

in which P, L denote the code and carrier-phase measurements in unit of meters; ρ indicates the geometrical distance between the antenna phase centers of satellite and receiver, which is calculated based on the known satellite orbit and approximate position of receiver; $\mathbf{g}$ is the unit directional vector from satellite to receiver antenna with a dimension of 1×3; $\mathbf{R}_n^e$ is the rotation matrix from n-frame to e-frame, which is constructed based on the approximate position of the receiver; $\mathbf{b}$ is a 3×1 column vector denoting the baseline vector expressed in n-frame; N means the double-differenced ambiguity parameters; ε indicates the double differenced code and phase measurement noises. One may note the satellite and receiver hardware delays are mitigated in (1).

2.3 Attitude representation

Determining the attitude of the bridge is calculating the rotation of b-frame with respect to the n-frame. Assuming $\boldsymbol{\theta}$ indicates the rotation vector from b-frame to n-frame and is represented in equivalent angle-axis format as $\boldsymbol{\theta} = \theta\mathbf{u}$ with $\theta = \|\boldsymbol{\theta}\|$ and $\mathbf{u} = \boldsymbol{\theta}/\theta$. Both direction cosine matrix and unit quaternions are commonly used in orientation representation in aerospace and robotics. Compared with the direction cosine matrix, the unit quaternion has the advantages of compact representation, smooth interpolation, avoidance of gimbal lock, and efficient rotation composition. There we are using quaternion to represent the orientation parameters, which is expressed as

$$\mathbf{q} = \begin{bmatrix} q_w \\ \mathbf{q}_u \end{bmatrix} = \begin{bmatrix} cos(\theta/2) \\ \mathbf{u}\, sin(\theta/2) \end{bmatrix}. \quad (2)$$

The relationship between the angle-axis rotation vector and the unit quaternion is briefly described as

$$\begin{cases} \theta\mathbf{u} \in \mathbb{R}^{\mathbf{3}} \xrightarrow{Exp(\cdot)} \mathbf{q} \in SO(\mathbf{3}) \\ \mathbf{q} \in SO(3) \xrightarrow{Log(\cdot)} \theta\mathbf{u} \in \mathbb{R}^{\mathbf{3}} \end{cases} \quad (3)$$

in which $Exp(\cdot): \mathbb{R}^3 \to SO(3)$ denotes an exponential map transforming the rotation vector to an equivalent unit quaternion; $Log(\cdot): SO(3) \to \mathbb{R}^3$ indicates the logarithmic map that project the unit quaternion to the equivalent rotation vector.

To derive the bridge attitude information, the baseline in n-frame ($\mathbf{b}_{r_1r_2}^n$) could be expressed as a function of unit quaternion as

$$\mathbf{b}_{r_1r_2}^n = F(\mathbf{q}) = \mathbf{q} \circ \mathbf{b}_{r_1r_2}^b \circ \mathbf{q}^{-1} \quad (4)$$

where $\circ$ is the operator of quaternion multiplication; $\mathbf{b}_{r_1r_2}^b$ represents the baseline vector of r_1r_2 in b-frame, which is precisely measured in advance and known. Substitute (4) into (1), then we get

$$\begin{cases} P_{r_0r_1,l}^{ij} = \rho_{r_0r_1}^{ij} + \mathbf{g}_{r_0}^{ij}\mathbf{R}_n^e\mathbf{b}_{r_0r_1}^n + \varepsilon\left(P_{r_0r_1,l}^{ij}\right) \\ P_{r_1r_2,l}^{ij} = \rho_{r_1r_2}^{ij} + \mathbf{g}_{r_1}^{ij}\mathbf{R}_n^e F(\boldsymbol{q}) + \varepsilon\left(P_{r_1r_2,l}^{ij}\right) \\ L_{r_0r_1,l}^{ij} = \rho_{r_0r_1}^{ij} + \mathbf{g}_{r_0}^{ij}\mathbf{R}_n^e\mathbf{b}_{r_0r_1}^n + \lambda_l N_{r_0r_1,l}^{ij} + \varepsilon\left(L_{r_0r_1,l}^{ij}\right) \\ L_{r_1r_2,l}^{ij} = \rho_{r_1r_2}^{ij} + \mathbf{g}_{r_1}^{ij}\mathbf{R}_n^e F(\mathbf{q}) + \lambda_l N_{r_1r_2,l}^{i} + \varepsilon\left(L_{r_1r_2,l}^{ij}\right) \end{cases} \quad (5)$$

Equation (5) is the measurement model for integrated positioning and attitude determination. Note that the measurement model is nonlinear because of the existence of nonlinear function $F(\mathbf{q})$ in (5). In the next section, we will introduce how to solve the equations based on UKF.

2.4 Integrated Positioning and Attitude Estimation

2.4.1 State representation

From (5), we can derive the nominal state vector as

$$\mathbf{X} = \begin{bmatrix} \underbrace{\mathbf{b}_{r_0r_1}}_{\mathbf{b}_{r_0r_1}\in\mathbb{R}^3} & \underbrace{\mathbf{q}}_{\mathbf{q}\in SO(3)} & \underbrace{\mathbf{N}}_{\mathbf{N}\in\mathbb{Z}} \end{bmatrix}^{\mathsf{T}}, \quad (6)$$

and its error state is formulated as

$$\boldsymbol{\delta}\mathbf{X} = \begin{bmatrix} \underbrace{\delta\mathbf{b}_{r_0r_1}}_{\delta\mathbf{b}_{r_0r_1}\in\mathbb{R}^3} & \underbrace{\delta\boldsymbol{\theta}}_{\delta\boldsymbol{\theta}\in\mathbb{R}^3} & \underbrace{\delta\mathbf{N}}_{\delta\mathbf{N}\in\mathbb{R}} \end{bmatrix}^{\mathsf{T}}. \quad (7)$$

The estimated state $\mathbf{X}$ is a point on the composite manifold $\mathcal{X} \triangleq \mathbb{R}^3 \times \mathbb{R}^{n_2} \times SO(3) \times \mathbb{Z}$. The error state $\delta\mathbf{X}$ is defined on the tangent space of $\mathcal{X}$ at $\mathbf{X}$, which can be parameterized with the vector space of float values.

Based on the state representation, the measurement model of (5) is further simplified in matrix format as

$$\mathbf{Y} = \mathbf{H}_1\delta\mathbf{b}_{r_0r_1} + \mathbf{H}_2F(\mathbf{q}) + \mathbf{H}_3\delta\mathbf{N} + \boldsymbol{\varepsilon}, \quad (8)$$

where the Observed-Minus-Computed (OMC) vector $\mathbf{Y}$, design matrices $\mathbf{H}_1$, $\mathbf{H}_2$, and $\mathbf{H}_3$ are constructed based on equation (5).

2.4.2 Propagation Step

The propagation step transforms the state and its variance-covariance through the kinematic model. The propagated state and covariance matrix from epoch $k-1$ to k is written as

$$\begin{cases}\mathbf{X}_{k|k-1} = \mathbf{F}_k\mathbf{X}_{k-1} + \omega_{k-1} \\ \boldsymbol{\mathcal{P}}_{k|k-1} = \mathbf{F}_k\boldsymbol{\mathcal{P}}_{k-1}\mathbf{F}_k^T + \mathbf{Q}_{k-1}\end{cases}, \tag{9}$$

where $\boldsymbol{\mathcal{P}}$ is the covariance matrix of the state vector; $\omega_{k-1} \sim \mathcal{N}(0, \mathbf{Q}_{k-1})$ is the process noise which follows a Gaussian normal distribution with a mean of 0 and a variance of $\mathbf{Q}_{k-1}$. $\mathbf{F}$ is the transition matrix, which could be a constant velocity model or IMU mechanization model with measurements of acceleration and angular rate. This work focusses on GNSS-only positioning and attitude determination, and the state propagation is modelled as a random walk process.

2.4.3 UKF update

The UKF simplifies nonlinear transformations by approximating the probability distribution rather than the function itself. It represents the state distribution as a Gaussian Random Variable (GRV) using a minimal set of sample points that accurately capture its mean and covariance. Propagating these points through a nonlinear system preserves the posterior mean and covariance up to the third order via the unscented transformation. To enhance numerical stability and reduce singularity risks, we propose an integrated positioning and attitude determination method based on UKF for SHM. Starting with the unscented transformation, the nonlinear measurement model of (8) is expressed in a function as

$$\begin{aligned}\mathbf{y}_{k|k-1} &= \mathcal{Y}(\mathbf{X}_{k|k-1}) \\ &= \mathbf{H}_1\delta\mathbf{b}_{r_0r_1,k|k-1} + \mathbf{H}_2F(\mathbf{q}_{k|k-1}) + \mathbf{H}_3\delta\mathbf{N}_{k|k-1}\end{aligned}. \tag{10}$$

To calculate the statistics of $\mathbf{y}_{k|k-1}$, we form a matrix $\mathbf{Z}$ with $2n_x + 1$ sigma vectors as

$$\begin{cases}\mathbf{Z}^0 = \mathbf{X}_{k|k-1} \\ \mathbf{Z}^i = \mathbf{X}_{k|k-1} \oplus \left(\sqrt{(n_x+\gamma)}\mathbf{S}_{\mathbf{X}_{k|k-1}}\right)_i, i \in (1 \cdots n_x) \\ \mathbf{Z}^j = \mathbf{X}_{k|k-1} \oplus \left(-\sqrt{(n_x+\gamma)}\mathbf{S}_{\mathbf{X}_{k|k-1}}\right)_{j-n^x}, j \in (n^x + 1 \cdots 2n_x)\end{cases}, \tag{11}$$

where n_x is the number of unknow parameters, $\mathbf{S}_{\mathbf{X}_{k|k-1}} = Chol(\boldsymbol{\mathcal{P}}_{k|k-1})$ is the square-root matrix of $\boldsymbol{\mathcal{P}}_{k|k-1}$, and calculated based on the Cholesky factorization. The operation $\oplus$ is defined as

$$\mathbf{X}_{k|k-1} \oplus \delta\mathbf{X} \triangleq \begin{bmatrix}\mathbf{b}_{r_0r_1,k|k-1} + \delta\mathbf{b}_{r_0r_1} \\ Exp(\delta\boldsymbol{\theta}) \circ \mathbf{q}_{k|k-1} \\ \mathbf{N}_{k|k-1} + \delta\mathbf{N}\end{bmatrix}. \tag{12}$$

The corresponding weights for calculating the mean value and covariance are defined as

$$\begin{cases}W_0^m = \gamma/(n_x+\gamma) \\ W_0^c = \gamma/(n_x+\gamma) + (1-\alpha^2+\beta) \\ W_i^m = W_i^c = 1/\left(2(n_x+\gamma)\right), i \in (1 \cdots 2n^x)\end{cases}. \tag{12}$$

where $\gamma = (\alpha^2 - 1)n_x$ is a scale parameter; The parameter α governs the dispersion of sigma points around $\mathbf{X}_{k|k-1}$. A practical rule of thumb suggests set $n_x + \gamma = 3$ when assuming $\mathbf{X}_{k|k-1}$ follows a Gaussian distribution (Julier et al., 2000). β serves to integrate prior knowledge regarding the distribution of $\mathbf{X}_{k|k-1}$, and $\beta = 2$ is considered optimal for Gaussian distributions (Wan and Van Der Merwe 2000). $\left(\sqrt{(n_x+\gamma)}\mathbf{S}_{\mathbf{X}_{k|k-1}}\right)_i$ denotes the i_{th} row of the matrix. The sigma vectors $\mathbf{Z}^i$, where i ranges from 0 to $2n_x$, undergo propagation via the nonlinear function (10), which are written as

$$\mathbf{y}_{k|k-1}^i = \mathcal{Y}(\mathbf{Z}^i), i \in (0 \cdots 2n_x). \tag{13}$$

Their weighted mean of the transformed observations is then calculated as

$$\bar{\mathbf{y}}_{k|k-1} = \sum_{i=0}^{2n_x} W_i^m \mathbf{y}_{k|k-1}^i. \tag{14}$$

The corresponding covariance (also known as innovation covariance) is computed through

$$\boldsymbol{\mathcal{P}}_{\mathbf{yy}} = \sum_{i=0}^{2n_x} W_i^c\left(\mathbf{y}_{k|k-1}^i - \bar{\mathbf{y}}_{k|k-1}\right)\left(\mathbf{y}_{k|k-1}^i - \bar{\mathbf{y}}_{k|k-1}\right)^\top + \mathbf{R}_k \tag{15}$$

The cross covariance between $\mathbf{X}_{k|k-1}$ and $\bar{\mathbf{y}}_{k|k-1}$ is calculated as

$$\boldsymbol{\mathcal{P}}_{\mathbf{Xy}} = \sum_{i=0}^{2n^x} W_i^c(\mathbf{Z}^i \ominus \mathbf{Z}^0)\left(\mathbf{y}_{k|k-1}^i - \bar{\mathbf{y}}_{k|k-1}\right)^\top, \tag{16}$$

and the corresponding operation of $\ominus$ is defined as

$$\mathbf{Z}^i \ominus \mathbf{Z}^0 \triangleq \begin{bmatrix}\mathbf{b}_{r_0r_1,k|k-1}^i - \mathbf{b}_{r_0r_1,k|k-1}^0 \\ Log\left(\mathbf{q}_{k|k-1}^i \circ \left(\mathbf{q}_{k|k-1}^0\right)^{-1}\right) \\ \mathbf{N}_{k|k-1}^i - \mathbf{N}_{k|k-1}^0\end{bmatrix}. \tag{17}$$

The UKF gain matrix $\mathbf{K}_k$ is then derived by solving the below equation

$$\mathbf{K}_k = \boldsymbol{\mathcal{P}}_{\mathbf{Xy}}\boldsymbol{\mathcal{P}}_{\mathbf{yy}}^{-1}, \tag{18}$$

The updated state vector is calculated as

$$\mathbf{X}_k = \mathbf{X}_{k|k-1} \oplus \left(\mathbf{K}_k\left(\mathbf{Y}_k - \bar{\mathbf{y}}_{k|k-1}\right)\right) \tag{19}$$

The posteriori covariances is then obtained as

$$\boldsymbol{\mathcal{P}}_k = \boldsymbol{\mathcal{P}}_{k|k-1} - \mathbf{K}_k\boldsymbol{\mathcal{P}}_{\mathbf{yy}}\mathbf{K}_k^\top \tag{20}$$

2.5 Ambiguity resolution

After we get the float solution, we need to resolve the estimates of float ambiguities to integers for improving the performances of positioning and attitude determination.

The estimated double-differenced ambiguities $\mathbf{N}$ and their covariance matrix $\boldsymbol{\mathcal{P}}_{\mathbf{N},\mathbf{N}}$ are seen as input arguments of the Least-Squares Ambiguity Decorrelation (LAMBDA) method (Teunissen 1995) to resolve the ambiguities, the resolved integer ambiguities is written as

$$\check{\mathbf{N}} = LAMBDA\left(\mathbf{N}, \boldsymbol{\mathcal{P}}_{\mathbf{N},\mathbf{N}}\right). \tag{21}$$

The position and attitude parameters with ambiguity resolution is then updated as

$$\begin{cases} \check{\mathbf{b}}_{r_0 r_1,k} = \mathbf{b}_{r_0 r_1,k} + \boldsymbol{\mathcal{P}}_{\mathbf{b},\mathbf{N}} \boldsymbol{\mathcal{P}}_{\mathbf{N},\mathbf{N}}^{-1} \left(\mathbf{N} - \check{\mathbf{N}}\right) \\ \check{\mathbf{q}}_k = Exp\left(\boldsymbol{\mathcal{P}}_{\boldsymbol{\theta},\mathbf{N}} \boldsymbol{\mathcal{P}}_{\mathbf{N},\mathbf{N}}^{-1} \left(\mathbf{N} - \check{\mathbf{N}}\right)\right) \circ \mathbf{q}_k \end{cases}. \tag{22}$$

where $\boldsymbol{\mathcal{P}}_{\mathbf{b},\mathbf{N}}$, $\boldsymbol{\mathcal{P}}_{\boldsymbol{\theta},\mathbf{N}}$ are submatrix extracted from $\boldsymbol{\mathcal{P}}_k$, denoting cross correlations between baseline vector $\mathbf{b}$, ambiguity $\mathbf{N}$, and rotation vector $\boldsymbol{\theta}$.

3 Dataset and configurations

In this paper, we utilize the dataset from the GeoSHM demonstration project (Meng et al., 2018), which was designed to develop an innovative system for monitoring large bridges, with the Forth Road Bridge in the UK serving as a case study. Specifically, we focus on data from two GNSS receivers mounted on the middle span of the bridge to evaluate the integrated positioning and attitude determination algorithm. The lateral and vertical displacements of the bridge are more sensitive to external factors such as wind and vehicle loads, leading to variations in roll and heading angles. Since a single baseline cannot determine 3D attitude, we constrain the pitch angle to zero degrees by setting its initial noise and process noise to zero in the UKF.

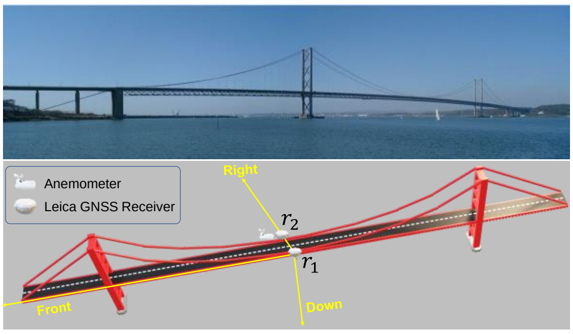

Figure 2. Forth road bridge and two GNSS receivers r_1, r_2 mounted on the middle span of the bridge

To test the algorithm under challenging conditions, we analyse data collected during a period of high wind speeds from January 2 to January 18, 2021, which caused significant lateral displacements of the bridge. The flowchart of data processing is illustrated in Figure 3. The data processing strategies are listed in Table 1.

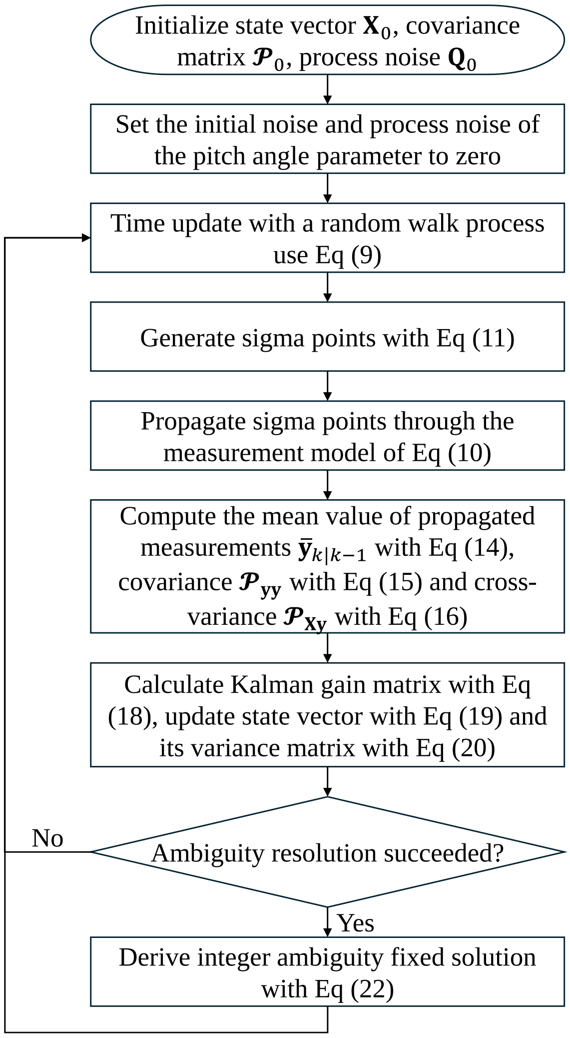

Figure 3. Flowchart of data processing

Table 1. Data processing strategies

Items	Processing strategies
GNSS signals	GPS: L1, L2 Galileo: E1, E5a
Sampling rate	10 s
Satellite orbit and clock	Broadcast ephemeris
Observation noise	0.6 m and 0.01 cycles for undifferenced code and phase measurements
Weighting strategy	Elevation angle dependent
Ambiguity resolution	The double-differenced ambiguities are resolved to integers by partial LAMBDA with a minimum success rate of 99.5% and ratio test with a threshold value of 3

4 Results and analysis

We use one base station r_0 and two monitoring r_1, r_2 to calculate the displacement of r_1 and determining the roll and heading of the middle span, as illustrated in Figures 1 and 2. For comparison, we use RTKLib (Takasu and Yasuda 2009) to calculate the bridge displacements and attitude. The displacement is derived from the RTKLib baseline solution r_0r_1, while the attitude is calculated as:

$$\begin{cases} roll = arcsin\left(\frac{\mathbf{b}^b_{r_1r_2,down}}{\|\mathbf{b}_{r_1r_2}\|}\right) \\ heading = arcsin\left(\frac{\mathbf{b}^n_{r_1r_2,east}}{\sqrt{\left(\mathbf{b}^n_{r_1r_2,east}\right)^2+\left(\mathbf{b}^n_{r_1r_2,north}\right)^2}}\right) \end{cases} \quad (22)$$

where $\mathbf{b}^b_{r_1r_2,down}$ is the down component expressed in b-frame for baseline r_1r_2; $\|\mathbf{b}_{r_1r_2}\|$ means the baseline length; $\mathbf{b}^n_{r_1r_2,east}$ and $\mathbf{b}^n_{r_1r_2,north}$ are east and north components expressed in n-frame.

4.1 Positioning performances

Figure 4 illustrates the lateral, longitudinal, and vertical displacements at the bridge's middle span, i.e. the point indicated as r_1 in Figure 1 and Figure 2. The corresponding wind speed data is plotted in Figure 5. The analysis reveals a strong correlation between the bridge displacements and wind speed. Structurally, the bridge exhibits higher stiffness in the longitudinal direction, resulting in longitudinal displacements that fluctuate randomly around zero with a standard deviation (STD) of 0.011 m. These longitudinal displacements are notably smaller compared to the lateral and vertical displacements.

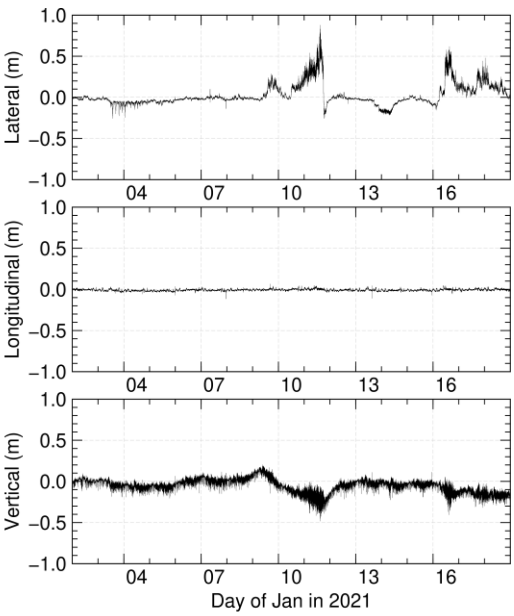

Figure 4. Lateral, longitudinal and vertical displacement at the bridge's middle span.

A comparison of Figures 4 and 5 reveals a strong correlation between wind speed variations and both lateral and vertical displacements. Notably, the cross-correlation in the lateral direction reaches 90.1%. From Figure 5, significant wind activity is observed on January 9–11 and January 16, corresponding to periods of large lateral and vertical displacements. Since the lateral wind speed is generally stronger than the vertical wind speed, the lateral displacements are also more pronounced than the vertical displacements during these periods.

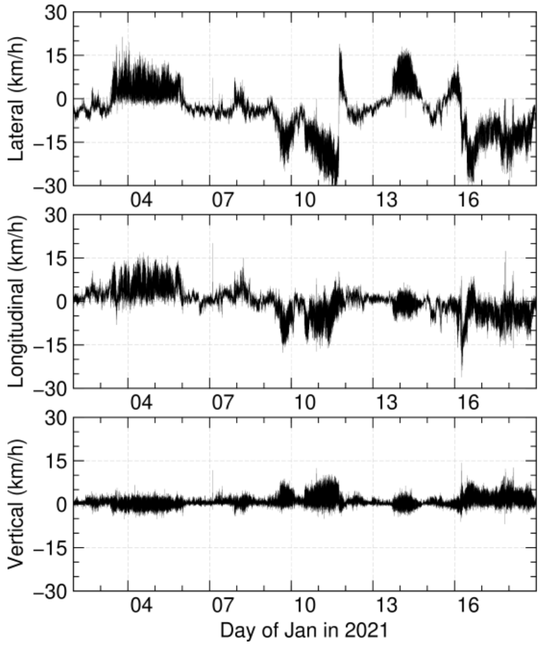

Figure 5. Wind speed in the lateral, longitudinal, and vertical directions at the bridge's middle span.

The positioning differences compared to the RTKLib solutions are presented in Figure 6. The RMS values for the lateral, longitudinal, and vertical components are 0.005 m, 0.009 m, and 0.015 m, respectively. The overall RMS values shown in Figure 6 represent the combined errors from both the integrated displacement and attitude determination (IDAD) solutions and the RTKLib solutions, which can be expressed as:

$$RMS_{overall} = \sqrt{RMS^2_{IPA} + RMS^2_{RTKLib}}, \quad (23)$$

where RMS_{IPA} and RMS_{RTKLib} denote the accuracy of the IDAD and RTKLib solutions, respectively Assuming the IDAD and RTKLib solutions have the equal accuracy, then we get: $RMS_{IPA} = RMS_{overall}/\sqrt{2}$. Therefore, the IDAD method can determine the bridge displacement with RMS values 0.004 m, 0.006 m and 0.011 m at lateral, longitudinal and vertical components.

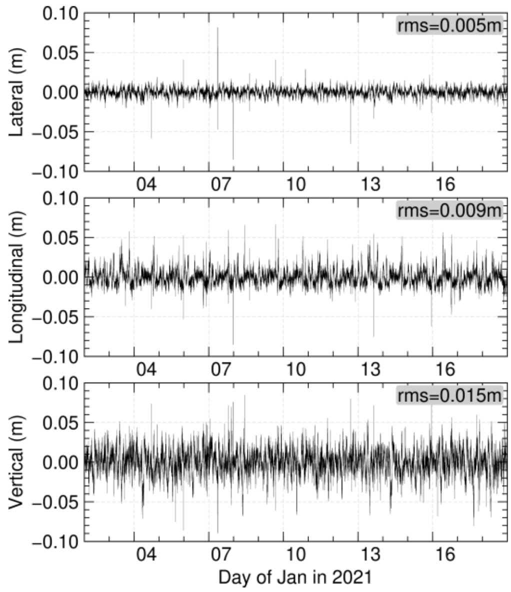

Figure 6. Positioning differences between the integrated positioning and attitude determination solutions and the RTKLib solutions.

4.2 Results of attitude determination

The bridge roll and heading variations are presented in Figure 7. When the large-span bridge is subjected to uneven external forces along its longitudinal direction (such as uneven wind force), it may experience longitudinal twisting. This process causes the bridge to rotate along its length, resulting in a change in the roll angle. Because of the strong wind occurred on January 11 and 16, we can see obvious roll angle fluctuations of 0.1 degrees. These fluctuations reflect small-scale side-to-side rotations of the midspan around the bridge's longitudinal axis.

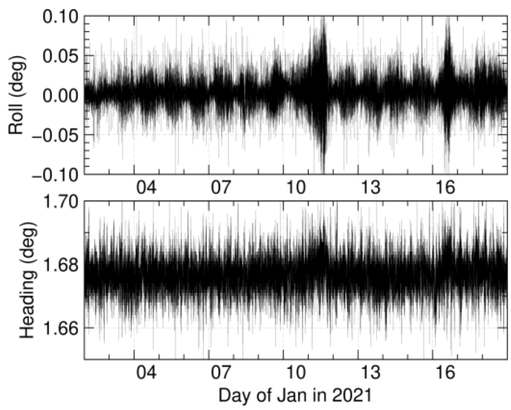

Figure 7. Determined roll and heading variations from January 2nd to 18th.

The bridge heading variation is also shown in Figure 7. The heading angle represents changes in the bridge's overall orientation, typically occurring when the bridge is subjected to lateral or oblique wind forces. These forces can induce rotational movement in the front and rear sections of the bridge, leading to variations in the heading angle. Although the variations are minimal, slight heading changes can still be observed on January 11 and 16, coinciding with periods of strong lateral winds.

Figure 8 illustrates the roll and heading differences between the IDAD solutions and RTKLib solutions. The calculated RMS values for the roll and heading angles are 0.008 degrees and 0.005 degrees, respectively. Similarly, we assume equal accuracy for the IDAD and RTKLib solutions, and apply the error propagation law from (23), it can be concluded that the IDAD method determines the roll and heading angles with accuracies of 0.006 degrees and 0.004 degrees, respectively. It is important to note that the accuracy of the estimated attitude also depends on the baseline length; a longer baseline results in higher attitude determination accuracy.

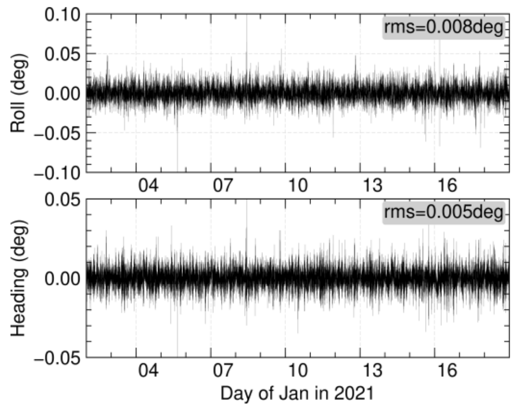

Figure 8. Roll and heading differences between the IDAD solutions and RTKLib solutions.

5 Conclusions and outlooks

Position and attitude information are critical for SHM of large bridges. GNSS-based integrated positioning and attitude determination is a complex nonlinear function. This contribution is the first to explore integrated positioning and attitude determination for SHM. We propose a simultaneous positioning and attitude determination method based on UKF. GNSS data collected from the Forth Road Bridge in the UK are used to evaluate the algorithm. The results demonstrate that the proposed method can estimate lateral, longitudinal, and vertical bridge displacements with accuracies of 0.004 m, 0.006 m, and 0.011 m, respectively, which are comparable to those from the classical RTK method. More importantly, it can simultaneously determine the bridge's attitude with accuracies of 0.006 degrees in roll and 0.004 degrees in heading. Both the estimated position and attitude can accurately reflect the displacement and attitude changes caused by strong wind in the test case.

In this study, the validation of GNSS-derived roll and heading results was primarily conducted through consistency checks with wind load variations. However, due to the unavailability of independent reference data, such as IMU or acceleration measurements, a direct quantitative validation was not feasible. Recognizing this limitation, we will deploy IMU sensors in the near future, enabling independent assessment of the GNSS-derived attitude solutions and further reinforcing the reliability of the proposed method.

Funding

This research is funded by the The National Nature Science Foundation of China (No. 42430711)

References

An, X., Bellés, A., Rizzi, F. G., Hösch, L., Lass, C., and Medina, D. (2024). Array ppp-rtk: A high precision pose estimation method for outdoor scenarios. *IEEE Transactions on Intelligent Transportation Systems*, 25(6), 6223-6237.

Brownjohn, J., Rizos, C., Tan, G. H., & Pan, T. C. (2004). Real-time long-term monitoring and static and dynamic displacements of an office tower, combining RTK GPS and accelerometer data. *The 1st FIG International Symposium on Engineering Surveys for Construction Works and Structural Engineering*. Nottingham, United Kingdom. 2004

Eling C., Klingbeil L., Wieland M., and Kuhlmann H. (2013a). A precise position and attitude determination system for lightweight unmanned aerial vehicles. *The International Archives of the Photogrammetry, Remote Sensing and Spatial Information Sciences*, Rostock, Germany.

Eling C., Zeimetz P., and Kuhlmann H. (2013b). Development of an instantaneous GNSS/MEMS attitude determination system. *GPS Solutions*, 17, 129-138.

Giorgi G., and Teunissen P. (2010) Carrier phase GNSS attitude determination with the multivariate constrained LAMBDA method. *2010 IEEE Aerospace Conference*, Big Sky, MT, USA.

Julier S., Uhlmann J., and Durrant-Whyte H. (2000) A new method for the nonlinear transformation of means and covariances in filters and estimators. *IEEE Transactions on Automatic Control*, 45(3): 477-482.

Liu, X., Ballal, T., Ahmed, M., and Al-Naffouri, T. Y. (2022). Instantaneous GNSS ambiguity resolution and attitude determination via Riemannian manifold optimization. *IEEE Transactions on Aerospace and Electronic Systems*, 59(3), 3296-3312.

Medina D., Vilà-Valls J., Hesselbarth A., Ziebold R., and García J. (2020) On the recursive joint position and attitude determination in multi-antenna GNSS platforms. *Remote Sensing*, 12: 1955.

Meng, X. (2002). Real-time deformation monitoring of bridges using GPS/accelerometers (Doctoral dissertation, University of Nottingham).

Meng, X., Nguyen, D. T., Xie, Y., Owen, J. S., Psimoulis, P., Ince, S., ... & Bhatia, P. (2018). Design and implementation of a new system for large bridge monitoring—GeoSHM. Sensors, 18(3), 775.

Takasu, T. and Yasuda, A. (2009) Development of the low-cost RTK-GPS receiver with an open source program package RTKLIB. IntI. Sym. on GPS/GNSS, Jeju, Korea, Nov. 2009.

Teunissen, P. (1995) The least-squares ambiguity decorrelation adjustment: a method for fast GPS integer ambiguity estimation. *Journal of Geodesy* 70: 65-82.

Teunissen, P. (2006). The LAMBDA method for the GNSS compass. *Artificial Satellites*, 41(3), 89-103.

Tian, Y., Sui, L., Wang, B., Dai, Q., Tian, Y., and Zeng, T. (2017). The Research on Nonlinear Attitude Determination Method of GNSS Multi-antenna Attitude Measurement. *In China Satellite Navigation Conference (CSNC) 2017 Proceedings*: Volume I (pp. 73-83). Springer Singapore.

Wan E. and Van Der Merwe R. (2000). The unscented Kalman filter for nonlinear estimation. *In Proceedings of the IEEE 2000 adaptive systems for signal processing, communications, and control symposium*, pp: 153-158.

Yu, J., Meng, X., Shao, X., Yan, B., and Yang, L. (2014). Identification of dynamic displacements and modal frequencies of a medium-span suspension bridge using multimode GNSS processing. *Engineering Structures*, 81, 432-443